WALAILAK JOURNAL

http://wjst.wu.ac.th Engineering and Physical Sciences

Entropy Generation for Peristaltic Blood Flow with Casson Model and Consideration of Magnetohydrodynamics Effects

Muhammad Mubashir BHATTI[1,*], Munawwar Ali ABBAS[2,3] and Mohammad Mehdi RASHIDI[4,5]

[1]*Shanghai Institute of Applied Mathematics and Mechanics, Shanghai University, Shanghai 200072, China*
[2]*Department of Mathematics, Shanghai University, Shanghai 200444, China*
[3]*Department of Computer Sciences, Karakoram International University, Skardu Campus, Gilgit Baltistan, Pakistan*
[4]*Shanghai Key Lab of Vehicle Aerodynamics and Vehicle Thermal Management Systems, Tongji University, Shanghai 201804, China*
[5]*ENN-Tongji Clean Energy Institute of Advanced Studies, Shanghai 200072, China*

([*]Corresponding author's e-mail: mubashirme@yahoo.com)

Received: 11 February 2016, Revised: 22 August 2016, Accepted: 30 September 2016

Abstract

In this article, entropy generation on peristaltic blood flow of the Casson fluid model is investigated under the influence of magnetohydrodynamics. The present mathematical analysis consists of continuity equations, momentum, and energy equations, which are simplified using the approximation of long wavelength and creeping flow regime. The reduced coupled differential equations are solved analytically, and a closed form of solution is presented. The impact of all the physical parameters of interest, such as the Brinkmann number, Hartmann number, and Casson fluid parameter, are taken into account. Trapping phenomena is also discussed with the help of contours. It is observed that the Casson fluid parameter and magnetic parameter show similar effects on velocity. Further, it is also observed that entropy profile behaves as an increasing function for all the pertinent parameters.

Keywords: Entropy, blood flow, magnetohydrodynamics, Casson fluid

Introduction

Over the last 2 decades, non-Newtonian fluid flow has appeared in many environmental and industrial applications. Bio fluids models have been investigated, by many researchers in various physiological systems, in order to deal with diagnostic problems, which arise during circulation of blood in the human body. Several models have been proposed by different authors based on physiological fluid; however, their full potential has not yet been exploited. Among these several models, the Casson fluid model is a special type of non-Newtonian fluid. This type of fluid is basically based on the interactive behaviour of the solid and liquid phases. Its behaviour depends upon shear stress rate; when shear stress is small, it acts like a solid, while it starts to move like a liquid when shear stress becomes higher than the applied yield stress. Some prominent examples of Casson fluid are fruit juice, jelly, tomato sauce, soup, honey etc. Casson [1] was the first to introduce the Casson fluid model. He derived a semi empirical equation for the flow behaviour of varnishes and printing inks. Later, Misra and Pandey [2] investigated the peristaltic transport of blood in small vessels by assuming blood as being a Casson fluid. They developed a mathematical model for blood flow in small vessels, and blood is treated as a 2 layer fluid where the core region is described by the Casson model. Recently, various researchers investigated the

Casson fluid model in different geometrical aspects [3-7]. One of the important characteristics of Casson fluid is that it is the most compatible formulation to simulate blood flow [8,9]. Biological organisms are composed of blood in vessels and extravascular tissue; blood flows into these organisms through arteries and perfuses the tissues via blood capillaries. Veins collect the returned blood from the capillaries, which is then pumped back to the heart. Also, through either a decrease in blood pressure or an increase in blood resistance, the flow rate of blood is reduced. Several authors investigated blood flow, theoretically and experimentally, by developing different kinds of models [10-12]. Pinho *et al*. [13] studied blood flow through micro vessels and microfluidic systems. They discussed the role of temperature on red blood cells dispersion.

Serious attention has been given by researchers to physiological systems, that is, fluids induced by a progressive wave of area expansion or contraction along the length of a distensible tube; this type of motion of fluid is called peristaltic motion. The mathematical model of peristaltic flow was first introduced by Latham [14] by taking the transport of urine, which moves from kidney to bladder. The occurrence of such motion can also be seen in blood pumps in the heart lung machine, chyme transport in the gastrointestinal tract, ovum movement in the female fallopian, and vasomotion of small blood vessels. Later, the pumping phenomenon of peristaltic flow in the ureter by using lubrication theory was studied by Carew and Padley [15]. After various investigations into peristaltic flow, several experimental and theoretical works have been reported [16,17]. Theoretical investigation of peristaltic flow of Williamson was reported by Nadeem and Akbar [18]. Moreover, peristaltic motion of magneto hydrodynamic (MHD), with certain problems of movement in physiological systems, is of great interest. Abbas *et al*. [19] discussed MHD peristaltic blood flow of Nano fluid in a non-uniform channel and derived the solution of temperature profile and concentration profile numerically as well as analytically. Sinha *et al*. [20] presented a theoretical study of MHD peristaltic flow and heat transfer in an asymmetric channel. A numerical solution of MHD peristaltic flow of a bio fluid in a circular cylindrical tube was studied by Ebaid [21]. It is quite possible that blood flow is influenced by the presence of magnetic fields because the red blood cell is a major bio magnetic substance. In addition, there are large numbers of Nano particles in blood, which are generally one thousand times smaller than a human hair, and the existence of these Nano particles cause many dangerous diseases, like blood cancer, etc. In most cases, traditional methods cannot be applied to remove these particles, but recently, Nano technology has been used to separate these particles from plasma [22]. According to this technology, magnetic fields can be used to separate drug-delivery nanoparticles from blood and pull them towards rings surrounding the chip's electrodes. Further investigations into MHD peristaltic flow are available in the list of references [23-27].

The studies mentioned above focus on peristaltic flow problems in the absence of entropy generation. Entropy generation can be expressed, as the various thermal systems are the subject of irreversibility phenomena, and are connected to viscous dissipation, magnetic field, and heat and mass transfer. Entropy generation clarifies energy losses in a system evidently in many energy related applications, such as the cooling of modern electronic devices or systems, geothermal energy systems. In the human body, oscillation of blood pressure is another important mechanism when patients conduct their normal routine work. Ambulatory blood pressure monitoring is also major clinical process to analyse blood pressure after every 20 - 30 min during 24 - 48 h. Further blood flow increases occur when the human body performs any physical activity, and in such kinds of situations blood circulation remains normal. When the temperature rises up to 20 °C, heat transfer takes place through the human body with the help of an evaporation process by sweating, whereas if it is less then 20 °C, the human body loses heat by conduction and radiation. To overcome this difficulty, entropy plays a major role in scrutinizing such systems. Few attempts have taken into account entropy generation on peristaltic flow. Akbar *et al*. [28,29] studied entropy and induced a magnetic field on the peristaltic flow of copper water fluid in an asymmetric horizontal channel and entropy generation on the peristaltic flow in a tube. Moreover, Rashidi *et al*. [30,31] investigated entropy generation on the MHD flow of third grade non-Newtonian fluid over a stretching sheet and MHD flow due to a rotating porous disk. Besides this, several researchers have analysed the irreversibility in systems and showed the pertinent parameters that might be chosen in order to minimize entropy generation [32-34].

From the above analysis, the aim of this study is to analyse the entropy generation on the peristaltic blood flow of the Casson fluid model under the influence of a magnetic field in a non-uniform channel. The governing flow problem is simplified with the help of long wavelength approximation and creeping flow phenomena. The resulting coupled differential equations are solved analytically, and exact solutions are obtained for velocity distribution and temperature distribution. This paper is summarized as follows; after the introduction in Sec. (1), Sec. (2) is based on the mathematical formulation, Sec. (3) characterizes the entropy generation analysis, while Sec. (4) describes the solution methodology and, finally, Sec. (5) is devoted to numerical results and discussion.

Mathematical formulation

Let us suppose the unsteady irrotational, hydromagnetic flow of a Casson fluid, which is incompressible and electrically conducting by an external magnetic field, "B_0" is applied through a 2-dimensional non-uniform channel having a sinusoidal wave moving down towards its walls. We have selected a Cartesian coordinate system for the channel in such a way that $\tilde{\boldsymbol{x}}$-axis is taken along the axial direction and $\tilde{\boldsymbol{y}}$-axis is taken along the transverse direction. The geometry of the governing flow problem can be described as;

$$\mathrm{H}(\tilde{x},\tilde{t}) = b(\tilde{x}) + \tilde{a}\sin\frac{2\pi}{\lambda}(\tilde{x}-\tilde{c}\tilde{t}), \tag{1}$$

where

$$b(\tilde{x}) = b_0 + \bar{K}\tilde{x},$$

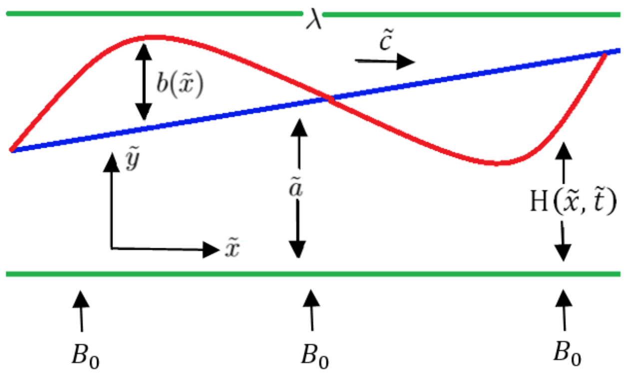

Figure 1 Geometry of the problem.

In the above equation, $b(\tilde{x})$ is the half width of the channel at any axial distance $\tilde{x}$ from inlet, b_0 is the half width at the inlet, $\bar{K}(\ll 1)$ is a constant whose magnitude depends on the length of the channel and exit inlet dimensions, $\tilde{a}$ is the wave amplitude, λ is the wavelength, $\tilde{c}$ is the velocity of the wave propagation, and $\tilde{t}$ is the time. The governing equation of motion, continuity and energy equation can be written as [19];

$$\frac{\partial\tilde{u}}{\partial\tilde{x}} + \frac{\partial\tilde{v}}{\partial\tilde{y}} = 0, \tag{2}$$

$$\rho\left(\frac{\partial\tilde{u}}{\partial\tilde{t}} + \tilde{u}\frac{\partial\tilde{u}}{\partial\tilde{x}} + \tilde{v}\frac{\partial\tilde{u}}{\partial\tilde{y}}\right) + \frac{\partial\tilde{p}}{\partial\tilde{x}} = \frac{\partial}{\partial\tilde{x}}\mathrm{S}_{\tilde{x}\tilde{x}} + \frac{\partial}{\partial\tilde{y}}\mathrm{S}_{\tilde{x}\tilde{y}} - \sigma B_0^2\tilde{u}, \tag{3}$$

$$\rho\left(\frac{\partial\tilde{v}}{\partial\tilde{t}}+\tilde{v}\frac{\partial\tilde{u}}{\partial\tilde{x}}+\tilde{v}\frac{\partial\tilde{v}}{\partial\tilde{y}}\right)+\frac{\partial\tilde{p}}{\partial\tilde{y}}=\frac{\partial}{\partial\tilde{x}}\mathrm{S}_{\tilde{y}\tilde{x}}+\frac{\partial}{\partial\tilde{x}}\mathrm{S}_{\tilde{y}\tilde{y}}-\sigma B_0^2\tilde{v}, \tag{4}$$

$$\zeta_0\left(\frac{\partial T}{\partial\tilde{t}}+\tilde{u}\frac{\partial T}{\partial\tilde{x}}+\tilde{v}\frac{\partial T}{\partial\tilde{y}}\right)=\frac{\kappa}{\rho}\left(\frac{\partial^2 T}{\partial\tilde{x}^2}+\frac{\partial^2 T}{\partial\tilde{y}^2}\right)+\frac{\mathrm{S}_{\tilde{x}\tilde{y}}}{\rho}\left(\frac{\partial\tilde{u}}{\partial\tilde{y}}\right). \tag{5}$$

The stress tensor of the Casson fluid model is defined as [3,4];

$$\tau^{1/n}=\tau_0^{1/n}+\mu\dot{\gamma}^{1/n}, \tag{6}$$

$$\tau_{i,j}=2e_{i,j}\left(\mu_b+\sqrt{2\pi_D}/\wp_y\right). \tag{7}$$

In the above equation, we have considered $\wp_y=0$. Now, it is convenient to define the non-dimensional quantities [19];

$$x=\frac{\tilde{x}}{\lambda},y=\frac{\tilde{y}}{b_0},t=\frac{\tilde{c}\tilde{t}}{\lambda},u=\frac{\tilde{u}}{\tilde{c}},v=\frac{\tilde{v}}{\tilde{c}\delta},p=\frac{\tilde{p}{b_0}^2}{\lambda\mu\tilde{c}},h=\frac{\mathrm{H}}{b_0},\phi=\frac{\tilde{a}}{b_0},\mathrm{Re}=\frac{\tilde{c}\rho\tilde{a}}{\mu},\delta=\frac{\tilde{a}}{\lambda},M=\sqrt{\frac{B^2\tilde{a}^2\sigma}{\mu}},\ v=\frac{\tilde{v}\tilde{a}\tilde{c}}{\lambda},\theta=\frac{T-T_0}{T_1-T_0},\mathrm{Pr}=\frac{v\zeta_0\rho}{\kappa},\mathrm{Ec}=\frac{\tilde{c}^2}{\zeta_0(T_1-T_0)},\mathrm{B_r}=\mathrm{Pr}\,\mathrm{Ec}. \tag{8}$$

where u,v are the non-dimensional axial and transverse velocity respectively, p is the dimensionless pressure, δ is the wave number, ϕ is the amplitude ratio, v is the fluid kinematic viscosity, θ is the dimensionless temperature, σ is the electrical conductivity of the fluid, Re is the Reynolds number, Pr is the Prandtl number, κ is the fluid thermal conductivity, ζ is the Casson fluid parameter, Ec is the Eckert number, $\mathrm{B_r}$ is the Brinkmann number, M is the Hartmann number, μ_b is the plastic viscosity, and Pr is the Prandtl number. Let us consider the creeping flow under the assumptions of long wavelength and low Reynolds number approximations. Using Eq. (8) in Eqs. (2) - (7) we get the resulting equations in simplified form as;

$$\left(1+\frac{1}{\zeta}\right)\frac{\partial^2 u}{\partial y^2}-M^2u=\frac{\partial p}{\partial x}, \tag{9}$$

$$\frac{\partial^2\theta}{\partial y^2}=-\mathrm{B_r}\left(1+\frac{1}{\zeta}\right)\left(\frac{\partial u}{\partial y}\right)^2, \tag{10}$$

Subject to the respective boundary conditions;

$$\frac{\partial u(0)}{\partial y}=0,\theta(0)=0, \tag{11}$$

$$u(h)=0,\theta(h)=1, \tag{12}$$

where $h=1+\frac{\lambda\bar{K}x}{b_0}+\phi\sin 2\pi(x-t)$. The above result reduces to a Newtonian fluid model by taking $\zeta\to\infty$.

Entropy generation analysis

The dimensionless volumetric entropy generation can be written as [32-36];

$$\mathbf{S}_{\mathbf{Gen}}'''=\frac{\kappa}{T_0^2}\left(\frac{\partial T}{\partial\tilde{y}}\right)^2+\frac{1}{T_0}\left[\mu\mathrm{S}_{\tilde{x}\tilde{y}}\left(\frac{\partial\tilde{u}}{\partial\tilde{y}}\right)+\sigma B_0^2\tilde{u}^2\right]. \tag{13}$$

The above equation in dimensionless form can be written as;

$$\boldsymbol{N_s} = \frac{\mathbf{S}'''_{\mathbf{Gen}}}{\mathbf{S}'''_{\mathbf{G}}} = \left(\frac{\partial\theta}{\partial y}\right)^{2} + \boldsymbol{\Lambda}\mathbf{B_r}\left(\mathbf{1} + \frac{1}{\zeta}\right)\left(\frac{\partial u}{\partial y}\right)^{2} + \boldsymbol{\Lambda}\mathbf{B_r}\boldsymbol{M^2 u^2}, \tag{14}$$

where

$$\mathbf{S}'''_{\mathbf{G}} = \boldsymbol{\kappa}\left(\frac{\boldsymbol{T_1} - \boldsymbol{T_0}}{\boldsymbol{T_0^2 b_0^2}}\right), \mathbf{B_r} = \frac{\tilde{c}^2 \mu T_0}{\kappa(T_1 - T_0)}, \boldsymbol{\Lambda} = \frac{T_0}{(T_1 - T_0)}. \tag{15}$$

Eq. (13) is divided into 2 groups. The first term in the entropy generation is due to the temperature difference, and the second part depicts the fluid friction irreversibility.

Solution of the problem

The solution of Eqs. (9) and (10) can be obtained by integrating twice, and thus we have;

$$u(y) = \frac{dp}{dx}\frac{1}{M^2}\left(\cosh\frac{My\sqrt{\zeta}}{\sqrt{\zeta+1}}\operatorname{sech}\frac{Mh\sqrt{\zeta}}{\sqrt{\zeta+1}} - 1\right), \tag{16}$$

$$\theta(y) = \frac{\left[4M^4 y\zeta - \mathrm{B_r}\left(\frac{dp}{dx}\right)^2 (h-y)\{-1+(-1+2hM^2 y)\zeta\} + \left\{y\left(4M^4\zeta + \mathrm{B_r}\left(\frac{dp}{dx}\right)^2(1+\zeta)\right)\cosh\frac{2Mh\sqrt{\zeta}}{\sqrt{\zeta+1}} - \mathrm{B_r} h\left(\frac{dp}{dx}\right)^2\cosh\frac{2My\sqrt{\zeta}}{\sqrt{\zeta+1}}\right\}\right]}{8hM^4\zeta\cosh^2\frac{Mh\sqrt{\zeta}}{\sqrt{\zeta+1}}}. \tag{17}$$

The instantaneous volume rate is defined as;

$$Q = \int_0^h u\mathrm{dy}. \tag{18}$$

$$Q = \frac{1}{M^3}\frac{dp}{dx}\left(\sqrt{\frac{\zeta+1}{\zeta}}\tanh hM\sqrt{\frac{\zeta}{1+\zeta}} - hM\right). \tag{19}$$

The pressure gradient (dp/dx) can be calculated from the above equation, and thus we have;

$$\frac{dp}{dx} = \frac{\sqrt{\zeta}M^3 Q}{\sqrt{\zeta+1}\left(\tanh hM\sqrt{\frac{\zeta}{1+\zeta}} - hM\sqrt{\frac{\zeta}{1+\zeta}}\right)}. \tag{20}$$

The non-dimensional form of the pressure rise $(\Delta \mathrm{P}_L)$ and along the wall with the length of the non-uniform channel L is given by;

$$\Delta\mathrm{P}_L = \int_0^{L/\lambda}\frac{dp}{dx}\mathrm{dx}. \tag{21}$$

Numerical results and discussion

In this section, the influence of different parameters of interest is investigated graphically. Computational software has been used to examine the novelties of all the pertinent parameters against the velocity profile, temperature profile, pressure rise, and entropy profile. To discuss the above results more vigorously, we assume that for instantaneous volume flow rate $Q(x,t)$ is periodic in $(x-t)$ and is defined by;

$$Q(x,t) = \bar{Q} + \phi\sin 2\pi(x-t), \tag{22}$$

where $\bar{Q}$ describes the average time flow over one period of the wave. **Figures 2 - 6** are plotted to show the expression of velocity distribution, pressure rise, temperature profile, and entropy generation for various parameters, such as the Hartmann number M, the Casson fluid parameter ζ, the Brinkmann number $\mathrm{B_r}$ and the temperature difference parameter Λ. **Figure 2** depicts the behavior of the velocity profile for the parameters M and ζ. It is observed that, with the increase in the Hartmann number $M\left(=\sqrt{\frac{B^2\tilde{a}^2\sigma}{\mu}}\right)$, the velocity profile decreases initially but starts to increase with the increase in y. Basically, the transverse magnetic field is introduced in the flow, due to the Hartmann parameter and, as a result, the Lorentz force generates and tends to resist the flow. Physically, a magnetic field is applied on the body to generate blood polarization and, with a magnetic field on the skin, a magnetic signal is received from electrodes in the blood. Similar behaviour of velocity distribution can be seen from **Figure 2(b)** for the Casson parameter ζ. Yield stress is inversely proportional to Casson fluid, and the increase in Casson parameter causes acceleration in a fluid flow. From **Figure 3(a)** it is noticed that pressure rise increases with the increase in Hartmann number M, but its reaction is opposite near the walls of the channel. Pressure rise decreases with the increase in Casson fluid parameter ζ, which can be analyzed in **Figure 3(b)**. Graphical behavior of pressure rise versus volume flow rate is plotted in **Figure 4**. It is revealed in **Figure 4(a)** that pressure rise increases in the retrograde pumping region ($\Delta P_L > 0$, $Q < 0$) when M increases, while decreasing behaviour can be found in the co-pumping region ($\Delta P_L < 0$, $Q > 0$) and the opposite response of pressure rise for Casson fluid parameter ζ is observed as shown in **Figure 4(b)**. **Figure 5** demonstrates the behavior of temperature profile and entropy generation for Brinkmann parameter $\mathrm{B_r}$. It is observed in both figures that, with the increase in $\mathrm{B_r}$, temperature profile and entropy generation increases. It is of true significance physically, since $\mathrm{B_r}(=\mathrm{Pr\,Ec})$ is a coefficient of fluid friction irreversibility (from Eq. (13)), and its increase raises fluid temperature through increase in viscous dissipation. The Brinkmann number is the product of the Prandtl number $\left(\frac{\nu\zeta_0\rho}{\kappa}\right)$ and the Eckert number $\left(\frac{\tilde{c}^2}{\zeta_0(T_1-T_0)}\right)$. The Prandtl number is described as the ratio of thermal to the momentum diffusivity, whereas the Eckert number is described as the conversion of kinetic energy in a channel/tube flow to heat through viscous dissipation. Temperature profile increases due to the increase in fluid temperature and, consequently, there is an increase in entropy generation. **Figure 6** shows that entropy generation is an increasing function of M and Λ. It is necessary to mention that there is a slight increase in entropy generation with an increase in magnetic parameter M. The reason behind this is that the magnetic parameter is not too much of an influence on entropy generation, so a large variation in M results in a small variation in entropy. It is depicted in **Figure 6(b)** that entropy profile increases significantly along the whole region for higher values of $\Lambda\left(=\frac{T_0}{(T_1-T_0)}\right)$. The next most engrossing part of this section is the trapping mechanism, which is plotted with the help of contours. It is a composition of internally moving bolus bounded by streamlines, called trapping. For this purpose, streamlines are drawn for different values of Hartmann number M and Casson fluid parameter ζ**.** It can be understood from **Figure 8** that, when the Hartmann number M increases, then the magnitude of the trapping bolus reduces, while the number trapping bolus also reduces. It can be observed from **Figure 9** that, when the Casson fluid parameter ζ increases, then the size of the bolus reduces slowly, while the number of bolus remains constant.

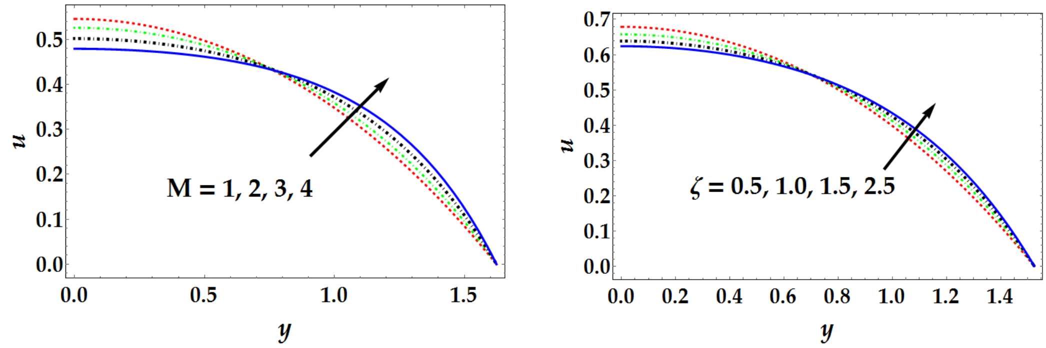

(a) (b)

Figure 2 Velocity distribution for various values of M and ζ when $\phi = 0.5, \bar{Q} = 0.1$.

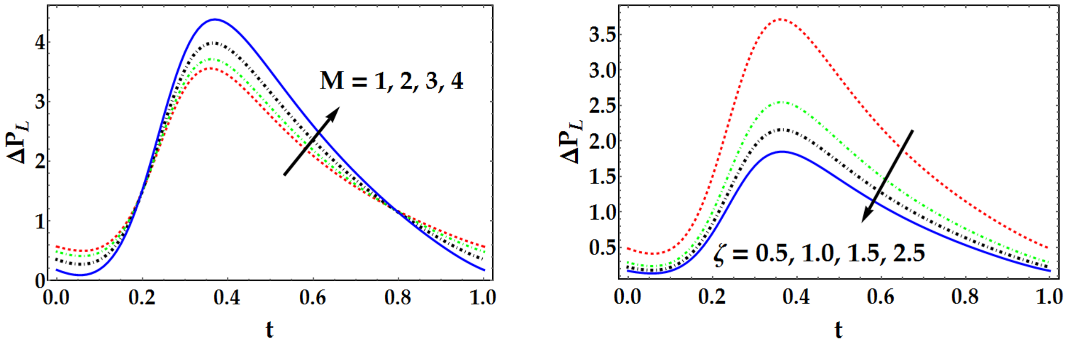

(a) (b)

Figure 3 Pressure rise for various values of M and ζ when $\phi = 0.5, \bar{Q} = 0.1$.

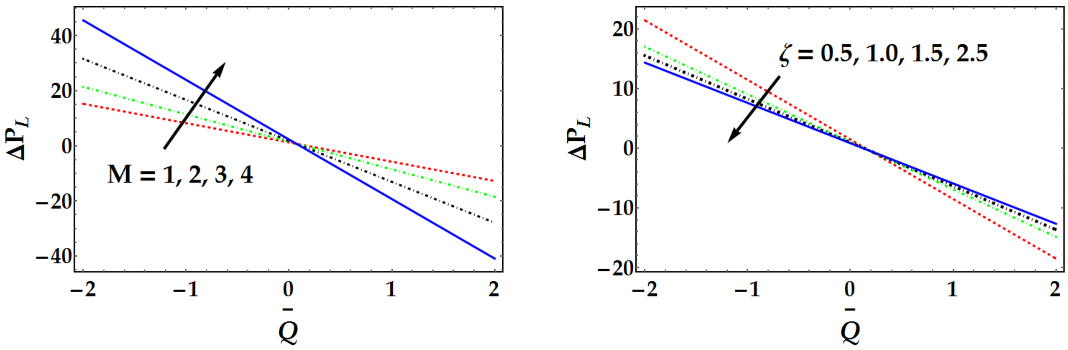

(a) (b)

Figure 4 Pressure rise *vs* average volume flow rate for various values of M and ζ when $\phi = 0.5$.

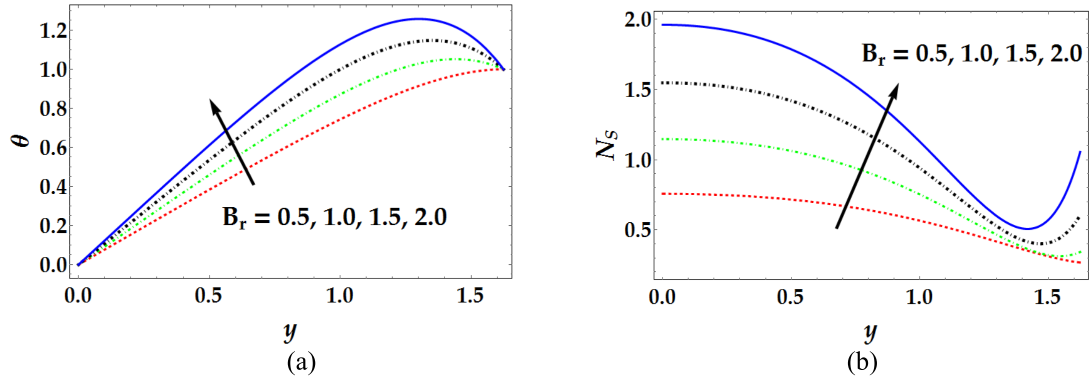

Figure 5 (a) Temperature distribution for various values of $\mathrm{B_r}$, (b) Entropy generation for various values of $\mathrm{B_r}$ when $\phi = 0.5, \bar{Q} = 0.1, \zeta = 0.5$.

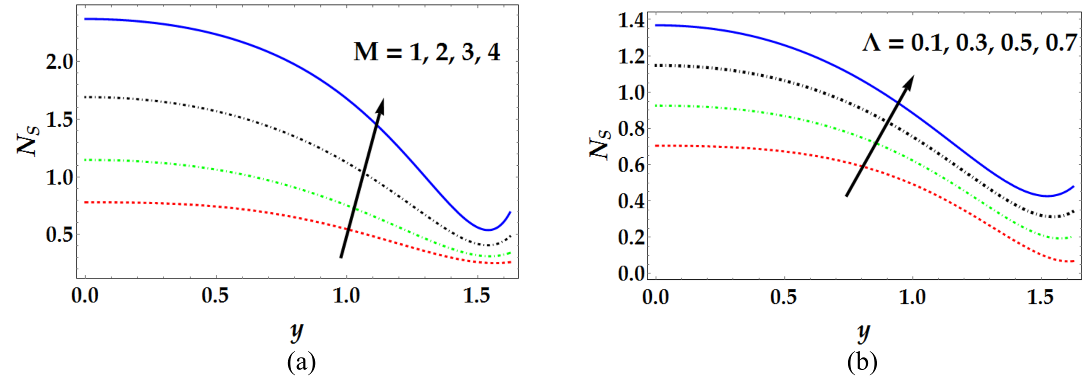

Figure 6 Entropy generation for various values of M and Λ when $\phi = 0.5, \bar{Q} = 0.1, \zeta = 0.5, \mathrm{B_r} = 1$.

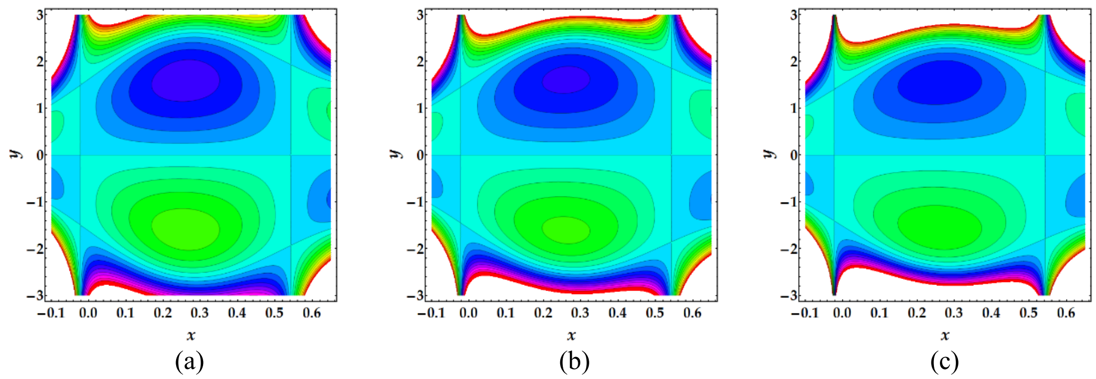

Figure 7 Stream lines for different values of M (a) 2, (b) 3, (c) 4, when $\phi = 0.5, \bar{Q} = 0.1,\ \zeta = 0.5$.

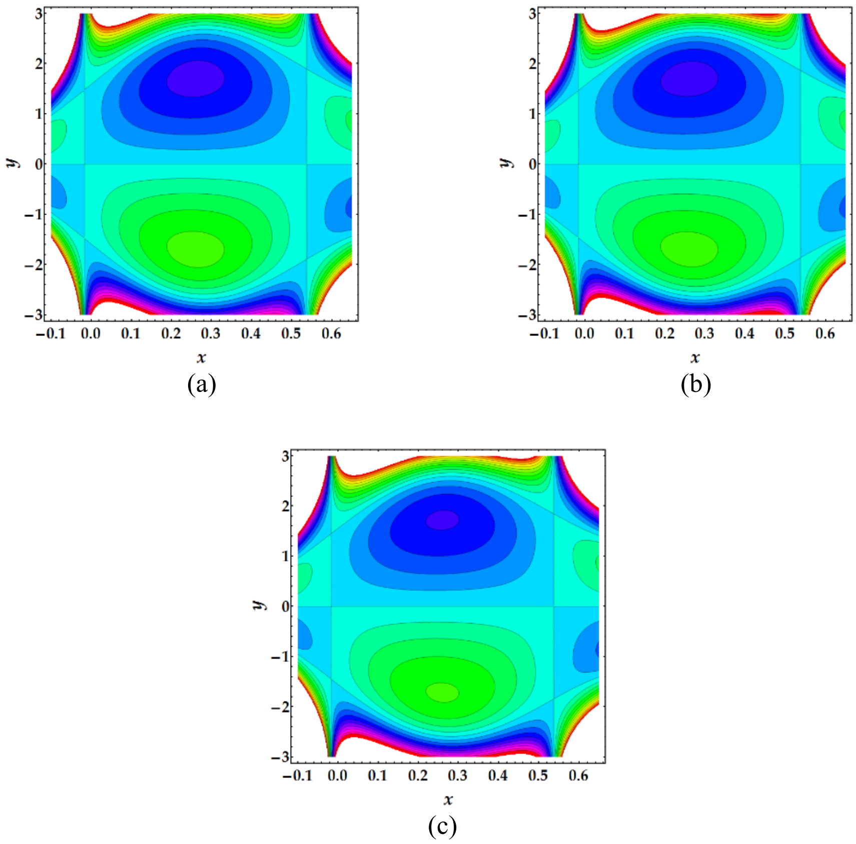

Figure 8 Stream lines for different values of ζ (a) 1, (b) 2, (c) 4, when $\phi = 0.5, \bar{Q} = 0.1, M = 2$.

Conclusions

In this article, entropy generation on the peristaltic blood flow of a Casson fluid model under the influence of MHD was studied. The governing flow problem was simplified with the help of long wavelength and creeping flow regime. The resulting ordinary coupled differential equations were solved analytically and the closed form solution was obtained. The effect of various pertinent parameters on temperature distribution, velocity distribution, pressure rise, and entropy profile were presented graphically with the help of the computational software Mathematica. The results obtained in this present analysis are as summarized below:

- When the Hartmann number (M) and Casson fluid parameter (ζ) increases, then the velocity profile shows the opposite behavior at the walls.
- Pressure rise increases for the Hartmann parameter (M), whereas the opposite response is shown for fluid parameter (ζ).
- It was observed that pressure rise versus volume flow rate increases with an increase in M, but it behaves as a decreasing function for fluid parameter (ζ).
- The behavior of entropy generation is increasing for all the physical parameters.
- The present analysis can also be reduced to Newtonian fluid by taking $\zeta \to \infty$.

References

[1] N Casson. *A Flow Equation for Pigment-Oil Suspensions of the Printing Ink Type*. Pergamon Press, Oxford 1959, p. 84-104.
[2] JC Misra and SK Pandey. Peristaltic transport of blood in small vessels: Study of a mathematical model. *Comput. Math. Appl.* 2002; **43**, 1183-93.
[3] S Akram and S Nadeem. Analytical analysis of peristaltic flow of a 6 constant Jeffreys model of fluid in an inclined planar channel. *Walailak J. Sci. & Tech.* 2014; **11**, 129-48.
[4] S Nadeem, RU Haq, NS Akbar and ZH Khan. MHD three-dimensional Casson fluid flow past a porous linearly stretching sheet. *Alexandria Eng. J.* 2013; **52**, 577-82.
[5] S Pramanik. Casson fluid flow and heat transfer past an exponentially porous stretching surface in presence of thermal radiation. *Ain Shams Eng. J.* 2014; **5**, 205-12.
[6] NS Akbar. Influence of magnetic field on peristaltic flow of a Casson fluid in an asymmetric channel: Application in crude oil refinement. *J. Magn. Magn. Mater.* 2015; **378**, 463-8.
[7] M Sheikh and Z Abbas. Homogeneous-heterogeneous reactions in stagnation point flow of Casson fluid due to a stretching/shrinking sheet with uniform suction and slip effects. *Ain Shams Eng. J.* 2017, DOI: 10.1016/j.asej.2015.09.010.
[8] KS Mekheimer. Peristaltic flow of blood under effect of a magnetic field in a non-uniform channels. *Appl. Math. Comput.* 2004; **153**, 763-77.
[9] KS Mekheimer and MAE Kot. The micropolar fluid model for blood flow through a tapered artery with a stenosis. *Acta Mech. Sinica* 2008; **24**, 637-44.
[10] KS Mekheimer and MAE Kot. Suspension model for blood flow through arterial catheterization. *Chem. Eng. Commun.* 2010; **197**, 1195-214.
[11] KS Mekheimer, MH Haroun and MAE Kot. Influence of heat and chemical reactions on blood flow through an anisotropically tapered elastic arteries with overlapping stenosis. *Appl. Math.* 2012; **6**, 281-92.
[12] SK Pandey and D Tripathi. Peristaltic transport of a Casson fluid in a finite channel: Application to flows of concentrated fluids in oesophagus. *Int. J. Biomath.* 2010; **3**, 453-72.
[13] D Pinho, RO Rodrigues, V Faustino, T Yaginuma, J Exposto and R Lima. Red blood cells radial dispersion in blood flowing through microchannels: The role of temperature. *J. Biomech.* 2015; **49**, 2293-8.
[14] TW Latham. Fluid Motions in a Peristaltic Pump. Ph.D. Dissertation, Massachusetts Institute of Technology, USA, 1966.
[15] EO Carew and TJ Pedley. An active membrane model for peristaltic pumping: Part I-Periodic activation waves in an infinite tube. *J. Biomech. Eng.* 1997; **119**, 66-76.
[16] R Ellahi, MM Bhatti and K Vafai. Effects of heat and mass transfer on peristaltic flow in a non-uniform rectangular duct. *Int. J. Heat Mass Trans*. 2014; **71**, 706-19.
[17] R Ellahi, MM Bhatti, C Fetecau and K Vafai. Peristaltic flow of couple stress fluid in a non-uniform rectangular duct having compliant walls. *Commun. Theor. Phys.* 2016; **65**, 66-72.
[18] S Nadeem and S Akram. Peristaltic flow of a Williamson fluid in an asymmetric channel. *Commun. Nonlinear Sci.* 2010; **15**, 1705-16.
[19] MA Abbas, YQ Bai, MM Rashidi and MM Bhatti. Application of drug delivery in Magnetohydrodynamics peristaltic blood flow of nanofluid in a non-uniform channel. *J. Mech. Med. Biol.* 2016; **16**, 1650052.
[20] A Sinha, GC Shit and NK Ranjit. Peristaltic transport of MHD flow and heat transfer in an asymmetric channel: Effects of variable viscosity, velocity-slip and temperature jump. *Alexandria Eng. J*. 2015; **54**, 691-704.
[21] A Ebaid. A new numerical solution for the MHD peristaltic flow of a bio-fluid with variable viscosity in a circular cylindrical tube via Adomian decomposition method. *Phys. Lett. A* 2008; **372**, 5321-8.

[22] S Ibsen, A Sonnenberg, C Schutt, R Mukthavaram, Y Yeh, I Ortac and MJ Heller. Recovery of drug delivery nanoparticles from human plasma using an electrokinetic platform technology. *Small* 2015; **11**, 5088-96.
[23] MM Bhatti, MA Abbas and MM Rashidi. Combine effects of Magnetohydrodynamics (MHD) and partial slip on peristaltic blood flow of Ree-Eyring fluid with wall properties. *Eng. Sci. Tech. Int. J.* 2016; **19**, 1497-502.
[24] MM Rashidi, MM Bhatti, MA Abbas and MES Ali. Entropy generation on MHD blood flow of nanofluid due to peristaltic waves. *Entropy* 2016; **18**, 117.
[25] MM Bhatti, R Ellahi and A Zeeshan. Study of variable magnetic field on the peristaltic flow of Jeffrey fluid in a non-uniform rectangular duct having compliant walls. *J. Mol. Liq.* 2016; **222**, 101-8.
[26] MA Abbas, YQ Bai, MM Bhatti and MM Rashidi. Three dimensional peristaltic flow of hyperbolic tangent fluid in non-uniform channel having flexible walls. *Alexandria Eng. J*. 2016, **55**, 653-62.
[27] S Akram, S Nadeem and A Hussain. Partial slip consequences on peristaltic transport of Williamson fluid in an asymmetric channel. *Walailak J. Sci. & Tech.* 2015; **12**, 885-908.
[28] NS Akbar, M Raza and R Ellahi. Peristaltic flow with thermal conductivity of H2O+ Cu nanofluid and entropy generation. *Results Phys.* 2015; **5**, 115-24.
[29] NS Akbar. Entropy generation analysis for a CNT suspension nanofluid in plumb ducts with peristalsis. *Entropy* 2015; **17**, 1411-24.
[30] MM Rashidi, S Bagheri, E Momoniat and N Freidoonimehr. Entropy analysis of convective MHD flow of third grade non-Newtonian fluid over a stretching sheet. *Ain Shams Eng. J*. 2017, **8**, 77-85.
[31] MM Rashidi, S Abelman and NF Mehr. Entropy generation in steady MHD flow due to a rotating porous disk in a nanofluid. *Int. J. Heat Mass Trans*. 2013; **62**, 515-25.
[32] OA Bég, MM Rashidi, N Kavyani and MN Islam. Entropy generation in hydromagnetic convective Von-Kármán swirling flow: Homotopy analysis. *Int. J. Appl. Math. Mech.* 2013; **9**, 37-65.
[33] MM Rashidi, L Shamekhi and S Kumar. Parametric analysis of entropy generation in off-centered stagnation flow towards a rotating disc. *Nonlinear Eng.* 2014; **3**, 27-41.
[34] R Ellahi, M Hassan, A Zeeshan and AA Khan. The shape effects of nanoparticles suspended in HFE-7100 over wedge with entropy generation and mixed convection. *Appl. Nanosci.* 2016; **6**, 641-51
[35] S Nadeem, A Riaz, R Ellahi, NS Akbar and A Zeeshan. Heat and mass transfer analysis of peristaltic flow of nanofluid in a vertical rectangular duct by using the optimized series solution and genetic algorithm. *J. Comput. Theor. Nanosci.* 2014; **11**, 1133-49.
[36] A Riaz, S Nadeem, R Ellahi and A Zeeshan. Exact solution for peristaltic flow of Jeffrey fluid model in a three dimensional rectangular duct having slip at the walls. *Appl. Bio. Biomech.* 2014; **11**, 81-90.